BRAIDING SIMULATION FOR RTM PREFORMS

R. Akkerman & B.H. Villa Rodríguez
University of Twente
Faculty of Engineering Technology,
P.O. Box 217, 7500AE, Enschede, NL
r.akkerman@utwente.nl

ABSTRACT
Braiding is a manufacturing process that is increasingly being used to manufacture pre-forms for Resin Transfer Moulding. A fast simulation method is presented for the prediction of the fibre distribution on complex braided parts and complex kinetic situations (e.g. changes in velocity, orientation). The implementation is suited for triangular surface representations as generated by many CAD software packages in use. Experimental results are presented to validate the model predictions, showing an acceptable correlation with the data predicted by the simulation method. The guide ring dimensions and spacing appear to have a significant effect on the accuracy of the predicted fibre orientations

INTRODUCTION
Automated braiding is a suitable process for manufacturing reproducible preforms for resin transfer moulding (RTM). It provides a fast fibre lay-down due to the simultaneous fibre deposition. The highly interlaced structure of braids makes it possible to cover components with sharp curvatures and non-circular cross-sections, varying along the length of the component. Furthermore, the interlaced nature of braids provides high levels of impact strength. Typical examples of these RTM components are propeller blades, trailing arms for a helicopter landing gear and automotive space frame components. So far, it was by no means trivial to predict the mechanical properties of an arbitrary braid reinforced product, firstly because the fibre directions could not be predicted in advance.

Most braid simulation models (1,2,3) are not suitable for the preforms indicated, with a non-axisymmetric cross-section, varying along the length of the component. Here, we will refer to these as ‘complex shapes’. Kessels and Akkerman (4) presented a model for the prediction of the yarn trajectories on these complex shaped mandrels, based on geometrical primitives (such as planar, cylindrical and spherical surfaces). A triangular surface mesh is a more versatile description, however, which is suitable for coupling to most CAD systems. This paper presents the algorithms, results, and experimental validation of such an implementation.

PROCESS DESCRIPTION
An illustration of a horn-gear braiding machine is given in fig.1. The mandrel, supported by a holder (not shown in the illustration), is located between the spools. The mandrel moves with an axial velocity, V. The yarns are driven by spools in the spool plane. One group of yarns, denoted as the warp yarns, moves clockwise while the weft yarns move counter-clockwise, both with an angular velocity of $\pm\omega$. The two yarn groups interlock, forming a closed biaxial fabric on the mandrel. Optionally a third group of yarns can be inserted through the horn gears (see fig.2). These stem yarns will be deposited in parallel to the mandrel axis, providing extra stiffness and strength in the axial direction of the now triaxially braided preform.

A pair of guide rings leads the yarns towards the mandrel. The yarns converge to the mandrel and touch the mandrel at a distance *H* from the guide ring. The point where a yarn touches the mandrel is denoted as the fell point. In operation, the mandrel with its holder can be driven to the right and left alternately for both forward and reverse braiding, and the layer of braid formed previously is covered (or 'overbraided') by the newly formed one. In this manner, multilayered products can be braided in one run.

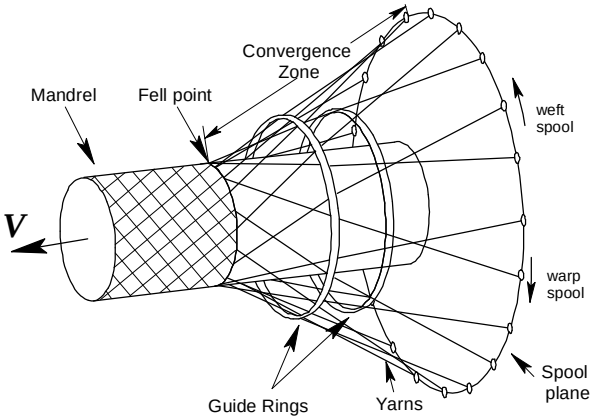

Figure 1. Braiding machine (schematically).

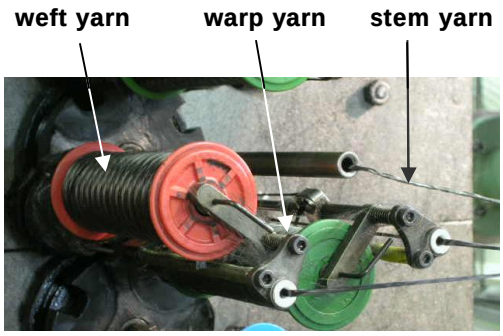

Figure 2. Yarn supply in the spool plane.

MATHEMATICAL MODEL

Fig.3 shows a model of a braiding machine with a complex mandrel. The frame of reference is chosen to be fixed to the mandrel. The yarn supply point, $\vec{q}$, is located on the guide ring in this case. The figure further shows the fell point of the yarn, $\vec{p}$, on the surface of the mandrel, *Q*, with for every point $\vec{x}$ on the surface:

$$Q(\vec{x}) = 0. \tag{1}$$

The angle between the path of the yarn and the tangent line of the surface in *z*-direction is the braid angle, α. The path of the yarn can be defined as a trajectory $\vec{f}(l)$ where the scalar l increases monotonically along the fibre path. The fell point, $\vec{p}(t)$, moves along this trajectory in time.

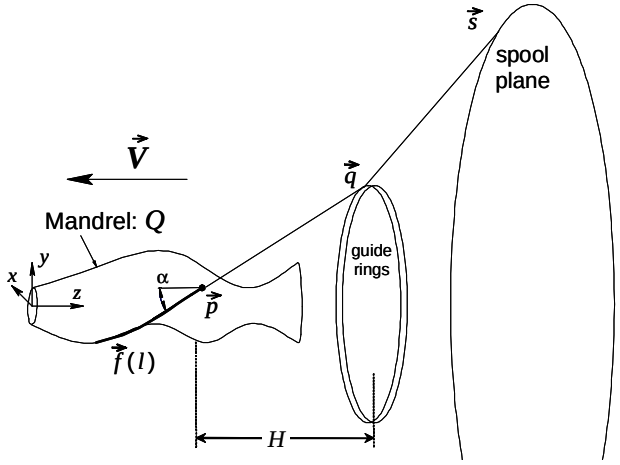

Figure 3. Model of a braiding machine with a complex mandrel.

Taking into account the conditions present in the manufacture of most of the braided RTM-preforms, the following assumptions were made to simplify the model without severely compromising the accuracy of the results:

1. There is no significant interaction between the fibres before they get in contact with the mandrel surface.
2. Fibres get totally interlocked once they are laid on the mandrel surface, thereby avoiding any re-arrangement in the fibre distribution.
3. The fibres lie exactly on the mandrel surface, i.e., there is no separation of the fibres from the mandrel.

Assumption 1 implies that it is sufficient to describe one single yarn at a time. The yarns are consequently straight in the free section in the convergence zone,

$$\vec{f}(g) = \vec{p}(t) + g \cdot (\vec{q}(t) - \vec{p}(t)); \qquad 0 \le g \le 1, \tag{2}$$

whereas assumption 2 states that fibre sliding is absent in the deposited zone,

$$\frac{\partial}{\partial t}\vec{f}(l) = 0; \qquad l \le l_p(t). \tag{3}$$

Assumption 3 can be represented as

$$Q\left(\vec{f}(l)\right) = 0; \qquad l \le l_p(t) \tag{4}$$

and thus the mandrel surface normal is normal to the yarn trajectory as well,

$$\frac{\partial}{\partial l}\vec{f}(l) \cdot \nabla Q\left(\vec{f}(l)\right) = 0; \qquad l \le l_p(t). \tag{5}$$

The yarn is continuous and differentiable at the fell point, where the free segment is connected to the deposited segment. This implies that the direction of the fibre path at the fell point, $\vec{p}$, has to be equal to the direction of the yarn path in the convergence zone. Hence eq.(5) leads to:

$$(\vec{p} - \vec{q}) \cdot \nabla Q(\vec{p}) = 0, \tag{6}$$

where of course the fell point is located on the mandrel surface,

$$Q(\vec{p}) = 0. \tag{7}$$

Equations (6) and (7) are to be solved for each fibre at every time step, with eqns.(2) and (3) as additional constraints.

DISCRETE APPROACH

We start from a triangular surface mesh, e.g. an STL representation or an FE mesh of the surface of the mandrel (fig.4). Each triangle is denoted as an element with nodes and edges connecting the consecutive nodes with a straight line. The sequence of node numbers

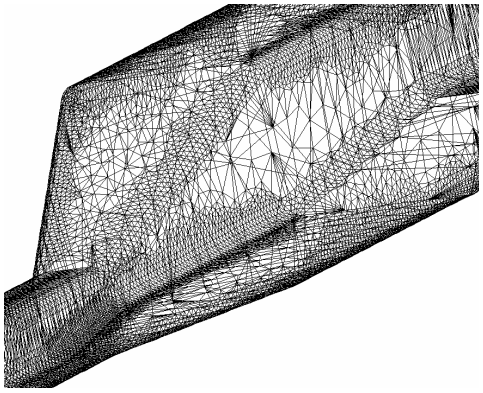

Figure 4. Triangular surface mesh of a mandrel surface.

connected to an element defines the normal vector of the element. The elements are numbered such that all element normals are pointing outwards.

The fibre path is defined as an array of points. These points are always located exactly at an element edge. A time stepping procedure is used, where the relative positions of the spool plane, the spools and the supply points are updated in every step.

The mandrel is supported by bars at both ends and clearly has a beginning and an end. Similarly, the surface mesh has edges. The starting edge is the one nearest to the spool plane. The fibre path is initiated by constructing the lines (two in case of a convex curve) from the supply point tangent to this edge. The appropriate intersection is chosen by considering the rotational direction of the spool. This is the start of the fibre path.

The fibre path is progressed in a stepwise manner. Consider the geometry in fig. 5. The current fell point $\mathbf{r}_{p}^{(j)}$ is known, as well as the edge on which the fell point is located, and the connected 'free element' ***abc*** where the fibre has not yet been deposited. The location of the supply point $\mathbf{r}_{q}$ changes due to the relative motion of the spools during a time step *Dt*. The line from the current fell point $\mathbf{r}_{p}^{(j)}$ to the new supply point $\mathbf{r}_{q}^{(j+1)}$ can be above or below the free element (based on the element normal). In the latter case, a new fell point can be determined.

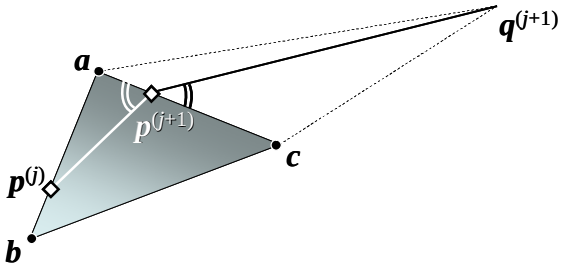

Figure 5 Location of the new fell point $\mathbf{r}_{p}^{(j+1)}$ between $\mathbf{r}_{p}^{(j)}$ and the supply point $\mathbf{r}_{q}^{(j+1)}$.

The new position will be on one of the two free edges (***ac*** and ***bc***) of the element. Zero friction is assumed at the moment of fibre deposition. This implies that there is no force exerted on the yarn tangent to the edge. Hence, there is a unique yarn path from the current fell point to the supply point passing over the line defined by an element edge. The angles between the yarn and the edge have to be equal on both sides of the edge, mathematically formulated as e.g.

$$\left\| \frac{\mathbf{r}_c - \mathbf{r}_a}{\|\mathbf{r}_c - \mathbf{r}_a\|} \times \frac{\mathbf{r}_p^{(j+1)} - \mathbf{r}_p^{(j)}}{\|\mathbf{r}_p^{(j+1)} - \mathbf{r}_p^{(j)}\|} \right\| = \left\| \frac{\mathbf{r}_c - \mathbf{r}_a}{\|\mathbf{r}_c - \mathbf{r}_a\|} \times \frac{\mathbf{r}_q^{(j+1)} - \mathbf{r}_p^{(j+1)}}{\|\mathbf{r}_q^{(j+1)} - \mathbf{r}_p^{(j+1)}\|} \right\|. \tag{8}$$

The solution is found iteratively. The new fell point is on the edge ***ac*** if this intersection is between the nodes $\mathbf{r}_{a}$ and $\mathbf{r}_{c}$. Otherwise the fell point will be on the edge ***bc*** where it can be determined likewise. The procedure is repeated for the new fell point, the corresponding edge and the free element until no further intersections of the yarn with the mandrel surface are found. The time stepping procedure ends when all fell points have reached the other end of the mandrel.

The supply point $\mathbf{r}_{q}$ was assumed to be in the perimeter of the guide ring in the previous implementation (4). For simplicity, the spools were treated as though they were turning on the guide ring instead of the spool plane. With complex mandrels, however, the supply point of a

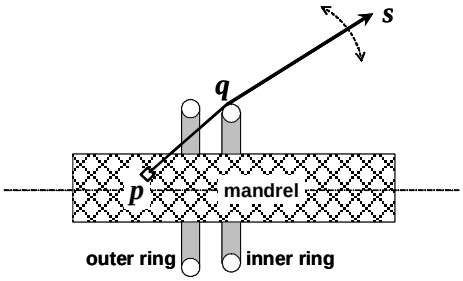

Figure 6. Position of the supply point ***q*** between the spool position ***s*** and the fell point ***p***.

yarn can vary from the inner to the outer ring or the spool itself (see fig. 6). The intersections of the straight line between the fell point and the spool with the guide ring planes are used to determine the appropriate supply point. A zero friction condition is used when the yarn is in contact with the guide ring.

The algorithms were implemented in C^{++} and a user friendly interface was added.

VALIDATION

A complex preform was used for validation purposes (see fig.7) as previously presented (4).

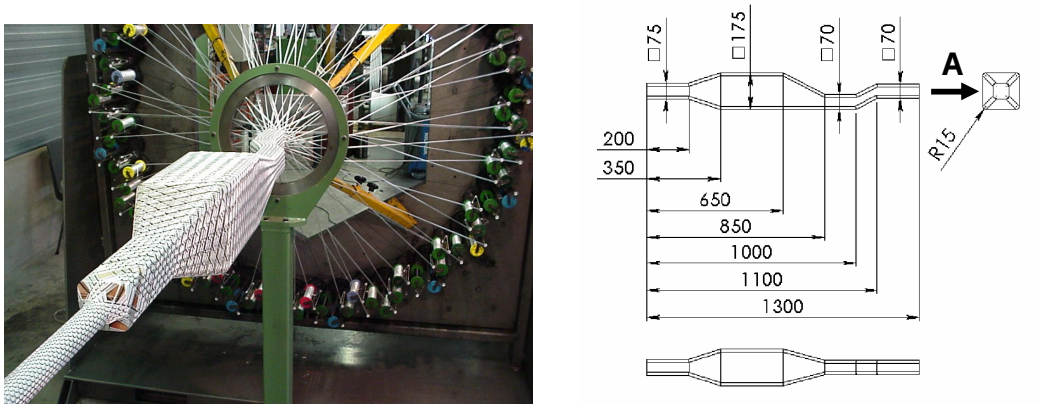

Figure 7. Validator mandrel; left: in the braiding machine, right: mandrel dimensions.

Eurocarbon's braiding machine was set up with the full set of 96 spools. Two types of warp and weft fibres were employed in order to simplify the fibre orientation measurements. A set of black polyester fibres (2×300 tex) was set at a regular separation in order to create a greater contrast with the remaining white glass fibres (1200 tex) and the mandrel surface.

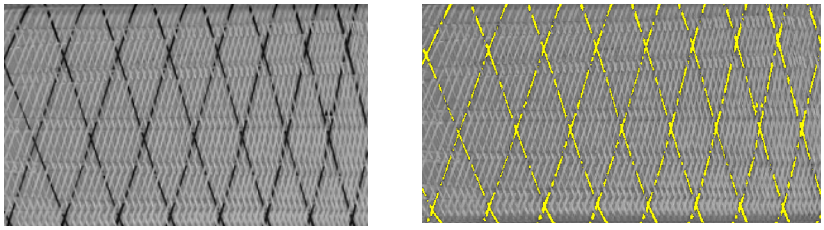

Figure 8. Image analysis using the highlighted yarns for fibre orientation measurement.

Experiments were performed with and without adhesive tape on the mandrel, in order to identify the effects of possible slip of the deposited yarns. The experiment with adhesive tape was performed twice. A constant axial velocity of 1 m/min and angular velocity of 0.628 rad/s were used in all cases. The black yarns were used for automated image analysis, as indicated in fig.8.

RESULTS AND DISCUSSION

The fibre angles were measured on the four faces for the warp and the weft yarns. The simulated fibre orientations were projected to the same plane of observation. The braiding experiments with adhesive tape (Test 2 and 3) show mutual differences of max 2º in braid angles. Fig. 9 illustrates the results for the weft yarn angle on face A in fig.7. Slip after deposition was not prohibited in Test 1, leading to an increased braid angle in the extension zone (200-350mm) and a decrease in the converging zone (650-850mm).

The process was simulated within a second on a middle class PC. The simulation results are generally within the experimental scatter. The deviation is larger in the regions where the supply point fluctuates between the guide rings. These results are particularly sensitive to the dimensions of and spacing between the guide rings. Regrettably, these were not recorded during the experiments and can only be estimated afterwards. It is possible to reduce the differences down to 2º by fine tuning the guide ring settings in the simulations.

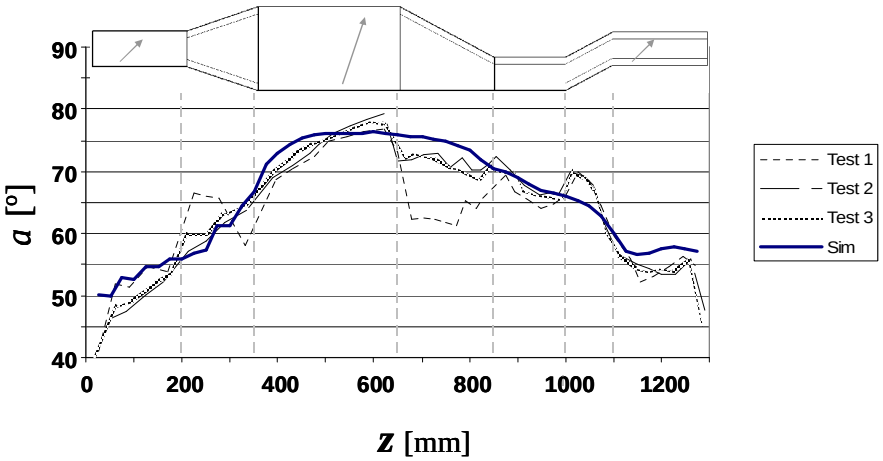

Figure 9. Braid angles (warp) vs *z*-coordinate on face A (fig.7): experimental and simulation results.

CONCLUSIONS AND RECOMMENDATIONS

A fast simulation model for braiding on arbitrary geometries was implemented in a user friendly software package. Braid angle predictions are accurate within the experimental scatter for complex mandrels with smooth geometry transitions. When the geometry transitions are more pronounced, the results are particularly sensitive to the guide ring settings, which require a more precise experimental validation. Fibre slip after yarn deposition leads to poor control of the braid angles. It inherently leads to deviations between experiment and simulation where this slip is ignored.

ACKNOWLEDGEMENT

The support of EuroCarbon B.V. and the Dutch National Aerospace Laboratory NLR is gratefully acknowledged.

REFERENCES

1. Ko F.K. 'Braiding' in: *Engineered Materials Handbook* **1**, ASM International, 519-528, 1987
2. Du G.W. and Popper P. *Journal of the Textile Institute* **85**:316-337 (1994)
3. Zhang Q., Beale D. and Broughton R.M. *J of Manufacturing Sci. and Eng.*, **121**:345-350 (1999)
4. Kessels, J.F.A. and Akkerman, R. *Composites Part A*, **33**: 1073-1081 (2002)